

## CONSTRAINTS ON THE GENESIS OF FERRIAN ILLITE AND ALUMINUM-RICH GLAUCONITE: POTENTIAL IMPACT ON SEDIMENTOLOGY AND ISOTOPIC STUDIES

HUGUES LONGUÉPÉE<sup>§</sup> AND PIERRE A. COUSINEAU

*Département des sciences appliquées, Université du Québec à Chicoutimi, Chicoutimi, Québec G7H 7J5, Canada*

### ABSTRACT

The term glauconite covers a series of iron-rich minerals that form in the upper layer of sediments of the sea bottom in locations where sediment input is low. Because of its potassium content and the process of its formation, it is one of few minerals that can be used in both sequence stratigraphy and in the determination of sedimentation age. Although aluminum-rich glauconite has been identified in several locations, the way it forms remains relatively unknown. A study of the ferrian illite from the Cambrian Anse Maranda Formation shows that, according to the present models for the formation of glauconite and diagenesis, the Al-for-Fe substitution responsible for the genesis of Al-rich glauconite occurs during early burial. In order to maintain charge balance while replacing Fe<sup>2+</sup> and Mg<sup>2+</sup> by Al<sup>3+</sup> at the octahedral site, there is an expulsion of K, as high as 31.6% of the measured K<sub>2</sub>O. This loss is important when evaluating the time needed to form glauconite and interpreting the occurrence of Fe-rich illite; it must be accounted for when using the K–Ar system, for either dating or in diagenetic studies.

*Keywords:* glauconite, glaucony, Fe-rich illite, diagenesis, mineral composition, Cambrian sedimentary units, Appalachians, Quebec.

### SOMMAIRE

La glauconite constitue une série de minéraux riches en fer qui se forment dans les couches de sédiment supérieures en milieu marin sous des conditions de faibles apports de sédiments. Comme elle contient du potassium et qu'elle se forme seulement à la surface des sédiments, la glauconite est un des rares minéraux qui peut être utilisé en stratigraphie séquentielle et pour déterminer l'âge de la sédimentation. Des échantillons de glauconite alumineuse ont été reconnus à travers le monde, mais le processus de formation demeure mal défini. Une étude de l'illite ferrugineuse de la Formation d'Anse Maranda, dans les Appalaches du Québec, suggère, selon les modèles actuels de formation de la glauconite et de diagenèse, que la substitution Al-pour-Fe responsable de la genèse de la glauconite alumineuse et de certains échantillons d'illite ferrugineuse se fait de façon précoce. Pour maintenir un équilibre des charges, le remplacement du Fe<sup>2+</sup> et du Mg<sup>2+</sup> par Al<sup>3+</sup> au site octaédrique s'accompagne d'une perte de K, qui peut atteindre 31.6% du K<sub>2</sub>O mesuré. Cette perte est importante lorsque vient le temps d'évaluer la maturité de la glauconite et l'origine de l'illite riche en fer. La perte en K est également un facteur à considérer dans l'interprétation du système K–Ar, que ce soit lors de datation ou d'une étude diagénétique.

*Mots-clés:* glauconite, glauconie, illite ferrifère, diagenèse, composition des minéraux, séquence cambrienne, Appalaches, Québec.

### INTRODUCTION

Glauconite, occurring as pellets or as a replacement of mineral grains and fossils, is composed of aggregates of micrometric crystals. An extensive literature has been devoted to glauconite because it is one of the few minerals that form exclusively in the uppermost layer of the sediment column (first meters of burial) in marine environments (Odin & Fullagar 1988, Odom 1984), where the rate of sedimentation is low (Odin & Matter

1981). Its formation involves different stages of growth that are reflected in K content, pellet morphology and crystalline structure (Odin & Matter 1981, Odin & Fullagar 1988). These stages have been set in a time frame by Odin & Fullagar (1988). The process leads to important variations of glauconite composition (Odin & Matter 1981, Odom 1976). Post-formational processes such as weathering (Huggett & Gale 1997, Odin & Fullagar 1988) and diagenesis (Dasgupta *et al.* 1990, Guimaraes *et al.* 2000, Ireland *et al.* 1983) have been

<sup>§</sup> *Current address:* Department of Earth Sciences, University of Ottawa, 140 Louis Pasteur, Ottawa, Ontario K1N 6N5, Canada.  
*E-mail address:* hlonguep@uottawa.ca

held responsible for some compositional variations in glauconite; among those, the occurrence of aluminum-rich glauconite has been of particular interest.

Here, we focus on a Cambrian glauconitic mineral from the Quebec Appalachians that has experienced above average Al-for-Fe substitution. Comparisons of the chemical composition of this glauconitic mineral and of glauconite throughout the world will be presented in an attempt to better identify the cause and intensity of the chemical changes that have led to this Al-rich composition. It is also an opportunity to verify if this substitution affects other chemical elements that form the mineral. The recognition of other variations in composition, particularly in potassium, is important because glauconite composition is used in detailed interpretations of sedimentary rocks (Odin & Fullagar 1988) and sequence stratigraphy (Amorosi 1997, Amorosi & Centineo 2000, Ruffell & Wach 1998). Finally, the influence of such compositional variations in glauconite on radiometric dating will be discussed.

#### BACKGROUND INFORMATION ON NOMENCLATURE ISSUES

The terms glaucony and glauconite are commonly found in the literature on sedimentary rocks. The term *glaucony* was introduced by Odin & Letolle (1980) to designate the grains and films formed by the process of glauconite formation and will be used as such. It is not a mineral name, but rather a morphological or facies term. The term *glauconite* has been used by sedimentologists to identify a potassium-rich (more than 8% K<sub>2</sub>O) green clay mineral found in the glaucony facies. Minerals in the same facies but with less potassium have been referred to with various names (Table 1). The nomenclature used by Amorosi (1997) is favored by sedimentologists because it links the differents

stages of evolution to the effective time of the process of glauconite formation.

According to the International Mineralogical Association (IMA), *glauconite* refers to a series of dioctahedral interlayer-deficient micas with a  $^{VI}Al / (^{VI}Al + ^{VI}Fe^{3+})$  value less than 0.5, a  $^{VI}R^{2+} / (^{VI}R^{2+} + ^{VI}R^{3+})$  greater or equal to 0.15, and with total interlayer cations between 0.6 and 0.85 per half unit cell (Rieder *et al.* 1998). The name for the glauconitic mineral with more than 0.85 interlayer cations is *celadonite*. Although the mode of origin should not be a criterion in mineral identification (Bailey *et al.* 1980), the environmental connotation of the name *celadonite* (associated to volcanic environments) is such that it has never been used to define a mineral found in the glaucony facies (marine sediments). Green clay minerals with 0.90 interlayers cations found in glaucony are still called glauconite by McCarty *et al.* (2004). This shows that the name glauconite has such a strong environmental meaning that it will take time to implement the proper use of the IMA nomenclature.

In this study, the term glauconite and celadonite are used according to the IMA classification. The terms glauconitic smectite is used for green clay minerals with less than 0.60 interlayer cations found in the glaucony facies. A comparison with other terminologies used in sedimentology research is given in Table 1.

#### SAMPLE PROVENANCE AND METHODOLOGY

Glauconitic minerals discussed in this study come from the Cambrian Anse Maranda Formation, near Quebec City, Canada. This formation, composed of bioturbated siliciclastic shelf sediments, contains 5 to 10% glauconitic minerals throughout its 355 meters thickness (Longu  p  e & Cousineau 2005). Diagenetic features include calcite cementation of burrows, and conversion of the feldspars to illite and chlorite. Rocks are not metamorphosed beyond this stage, but were buried to the dry gas zone (Bertrand, written commun., 2002). The interest in this formation lies in 1) the unusual thickness of its glauconite-rich interval (Amorosi 1997), 2) its status as the only glauconite-rich formation in the northern Appalachians, and 3) the age of the formation, poorly constrained until recently. Knowledge of the true mineralogical nature of these green pellets also is necessary for further interpretation of depositional settings and possible radiometric dating.

In order to determine the habit, mineralogy and chemistry of the glauconitic mineral, several analytical methods were used. The shape and distribution of the grains were observed in outcrop, hand specimens and thin sections. The mineralogy of the green pellets was determined by powder X-ray diffraction. Rock samples were crushed into fragments smaller than 1 cm and then placed in 250 mL Nalgene bottles with stainless steel balls and 125 mL of distilled water. The bottles were

TABLE 1. NOMENCLATURE OF GLAUCONITIC MINERALS ACCORDING TO THE IMA, AND EQUIVALENT TERMS USED IN SEDIMENTOLOGY-RELATED PAPERS

Interlayer <i>apfu</i>	Rieder <i>et al.</i> (1998)	K <sub>2</sub> O wt. %	Odin & Matter (1981)	Amorosi (1995)	Cristallinity
<0.6	Glauconitic smectite	<4	Glauconitic smectite	Nascent glaucony	Smectite
<0.6	Glauconitic smectite	4-6	Glauconitic mineral	Slightly evolved glaucony	
0.6-0.85	Glauconite	6-8	Glauconitic mineral	Evolved glaucony	
>0.85	Celadonite	>8	Glauconitic mica	Glauconite	Mica

The IMA divisions (Rieder *et al.* 1998) are based on interlayer cations /  $O_{10}(\text{OH})_2$ , whereas other classifications are based on K<sub>2</sub>O content. The term "glauconitic smectite" is not part of the IMA classification, but it is used here to represent glauconitic minerals with less than 0.6 interlayer cations per formula unit (*apfu*).

shaken for one hour using a paint shaker to further reduce the size of the particles without changing the clay mineral structurally by heating. Samples were acid-treated (HCl, 10%) at room temperature for about two minutes to eliminate any carbonate cement. The particles were then rinsed using de-ionized water, dried and sieved to keep only the 63–500  $\mu\text{m}$  fraction. Green pellet concentrates were obtained using a Frantz magnetic separator. A 20° slope, 15° lateral tilt and 0.6 mA current were found to give optimal results. These settings are similar to those used by Amorosi (1993). The pellet concentrates were further reduced in size with an agate mortar. Ultrasonic disaggregation was attempted but was not successful. Finally, samples of particles less than 10  $\mu\text{m}$  were obtained by centrifuging. The X-ray-diffraction data were acquired with a Philips PW1050 diffractometer operating with  $\text{CuK}\alpha$  radiation and a scan speed of 1°/min from 5° to 60° (2 $\theta$ ). Oriented, glycol-solvated, as well as non-oriented samples were analyzed.

The chemical composition of the green pellets was determined using a Cameca SX-100 electron microprobe at Laval University. Points were analyzed with a 5  $\mu\text{m}$  beam (intensity of 20 nA) with counts for 20 seconds on the peaks, and 10 seconds for the background. The major oxides were determined for a total of 13 samples (with two or three analyzed pellets). There is no significant loss in potassium in the phyllosilicate minerals caused by beam volatilization with the operating conditions selected (M. Choquette, pers. commun., 2003). Samples AM-02C, AM-04A and

PG-1-2A were analyzed for ferrous iron by the titration method of Wilson (1955) as modified by Whipple (1974).

#### PETROGRAPHY OF THE GREEN PELLETS

Petrographic studies of the Anse Maranda Formation sandstones show that the green pellets are formed from aggregated micrometric clay grains. Their shape, green color and high birefringence are typical of glauconitic minerals. Whereas one cannot confirm the exact composition of the pellets with petrography, this approach yields spatial and temporal characteristics, so that one can ascertain if they are autochthonous or allochthonous. This distinction is crucial for the interpretation of glauconite-bearing rocks (Amorosi 1995). Although there is no single definitive criterion, there are various characteristics for autochthonous and allochthonous glauconite (Amorosi 1997, Hesselbo & Huggett 2001, Huggett & Gale 1997, McCracken *et al.* 1996). The two characteristics that strongly suggest the autochthonous nature of the glauconite are the high concentration of pellets within burrows compared to beds of the host sediments and the occurrence of fractures called “*craquelures*” (Lamboy 1976). “*Craquelures*” (Fig. 1a) are brittle features that typically would not resist long transport; therefore, their presence is indicative of *in situ* growth. The uniform distribution of glauconitic pellets throughout the entire Anse Maranda Formation, and also within individual beds (*i.e.*, no concentration along specific laminae), is an indication that the grains were

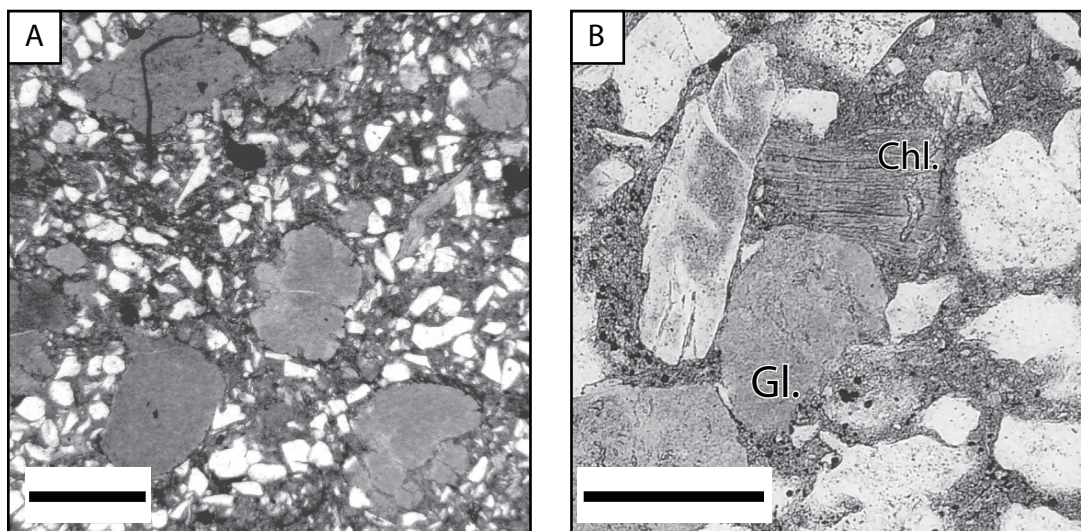


FIG. 1. A) Typical glauconitic pellet of the Anse Maranda Formation showing autochthonous characteristics such as “*craquelures*” and a large size compared to the surrounding matrix. In some part of the formation, these pellets are concentrated in burrows, suggesting glauconite formation at the expense of fecal pellets. B) Glauconite pellets and tabular chlorite with well-developed cleavage. Iron oxides are occasionally found along the cleavage. Scale bar is 500  $\mu\text{m}$ .

neither transported nor sorted by currents. The occurrence of glauconitic pellets twice the grain size of the host sediments can also be attributed to *in situ* growth. In most cases, the Anse Maranda Formation glauconitic pellets are at least twice as large as the quartz or feldspar grains (Fig. 1a). Hydraulic equivalence cannot explain such a difference in grain size. The recognition of the autochthonous nature is important because it allows the burial and diagenetic history of this mineral to be deduced from other features within the host formation. Furthermore, dating defines the true age of the host sediment, not the age of the source.

#### MINERALOGY OF THE GREEN PELLETS

The diffraction data of most samples of green pellets from the Anse Maranda Formation show the presence of two minerals (Fig. 2). The first mineral is a glauconite (or illite) easily identified using the 00 $l$  reflections in the oriented samples, with the 00 $l$  at 10.4 Å. The glycol-solvated sample shows a slight shift in

the 00 $l$  reflection to 10.3 Å, which suggests a small amount of interstratification. This is common, as the glauconite structure gradually evolves unevenly from smectite to mica (Odin & Matter 1981). The position of 002/003 illite/smectite reflection at 17.7° on the glycol-solvated diffraction pattern (Fig. 2) suggests that the pellets contain more than 90% of 10 Å layers and that the Reichweite number (R) equals 3 (Moore & Reynolds 1989). In pellets where potassium is the lowest (see below), the glauconite is still composed of more than 80% of 10 Å layers. The 002 reflection is of higher intensity than it should be for a glauconite. This is explained by an aluminum-for-iron substitution in the octahedral site (see below).

The second mineral shows an 060 reflection for non-oriented samples indicative of a trioctahedral mineral. It is interpreted to be an iron-rich chlorite on the basis of a weak reflection at 14 Å and a strong one at 7 Å for oriented samples. This was confirmed by electron-microprobe analysis. This mineral is easily identified in thin section, as it occurs as tabular grains with a

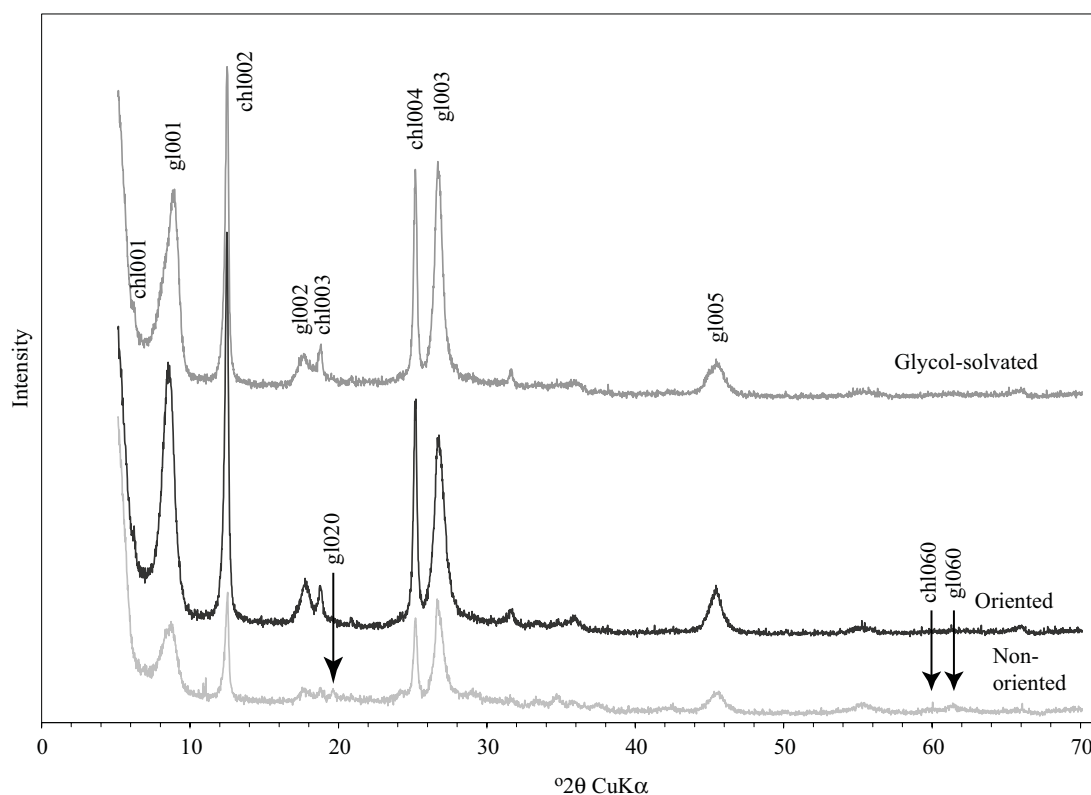


Fig. 2. X-ray-diffraction patterns of green clay minerals from the glaucony facies (sample PG-1-2A). There is a minimal shift in the 00 $l$  reflection of glauconite (illite) from 10.4 to 10.3 Å between oriented and glycol-solvated samples, which suggest the presence of a few % of smectite layers. A very small peak at 60°2θ and relative intensities of (00 $l$ ) reflections enabled the identification of an iron-rich chlorite, easily recognizable in thin section and visible in Figure 1.

well-defined cleavage (Fig. 1b) and is not part of the green pellets. It is found with glauconite on XRD results merely because of the difficulty of separating the two during sample preparation. The XRD data suggest that the chlorite is iron-rich and of the Ib polytype. The Ib polytype indicates that this chlorite is likely authigenic or diagenetic.

#### CHEMICAL COMPOSITION OF GLAUCONITIC PELLETS

The chemical composition within a glauconitic pellet is generally heterogeneous because of the complex process of its formation (Odin & Matter 1981). Variations from rim to center in the glauconite pellets from the Anse Maranda Formation are small (Table 2). The average composition within a pellet on which a transect was done (Table 3) is not significantly different from the

composition of pellets on which only two measurements were taken (Table 4).

Potassium in the glauconite of the Anse Maranda Formation varies from 5.85 to 8.62% K<sub>2</sub>O. An important characteristic of the glauconitic mineral is that it contains more aluminum than iron. Although measurement of ferrous iron is not precise because of small amounts of chlorite in the three samples used for measurements by iron titration, the Fe<sup>2+</sup> : Fe<sup>3+</sup> ratio is close to 0.25. This is slightly lower than 0.30, the value measured for other samples of aluminum-rich glauconite (Ireland *et al.* 1983). The 0.25 value was applied to all "glaucony" compositions (Table 4), and stoichiometric formulas were calculated on the basis of 10 atoms of oxygen and two hydroxyl groups (22 layer charges). Using the IMA classification (Rieder *et al.* 1998), the mineral forming the green pellets in the

TABLE 2. CHEMICAL COMPOSITION ACROSS A PELLET TAKEN FROM SAMPLE AM-02C

	Rim		Center						Rim		Ave.	σ
	1	2	3	4	5	6	7	8	9	10		
SiO <sub>2</sub> wt.%	53.87	52.39	54.34	54.22	53.52	52.37	53.20	52.07	51.64	51.24	52.89	1.10
TiO <sub>2</sub>	0.09	0.10	0.08	0.09	0.09	0.07	0.10	0.10	0.08	0.11	0.09	0.01
Al <sub>2</sub> O <sub>3</sub>	21.03	20.80	20.71	20.47	20.33	19.97	20.09	20.01	19.68	22.58	20.57	0.82
MgO	2.37	2.41	2.37	2.41	2.36	2.42	2.41	2.36	2.49	2.43	2.40	0.04
CaO	0.09	0.06	0.10	0.06	0.07	0.09	0.07	0.06	0.07	0.08	0.07	0.01
Fe <sub>2</sub> O <sub>3</sub>	8.44	8.63	8.51	8.83	8.64	9.69	8.98	9.33	9.76	7.65	8.84	0.63
FeO	1.92	19.96	1.94	2.01	1.96	2.20	2.04	2.12	2.22	1.74	2.01	0.14
Na <sub>2</sub> O	0.13	0.15	0.13	0.13	0.16	0.13	0.13	0.13	0.12	0.14	0.14	0.01
K <sub>2</sub> O	7.97	8.38	8.19	8.12	8.18	8.28	8.28	7.85	8.35	8.20	8.18	0.17

This pellet shows the greatest variation in the Anse Maranda Formation. Analysed points are 9 μm apart. Note the lower values of K and Fe and higher values of Al at the margin of the pellets.

TABLE 3. AVERAGE COMPOSITION OF GLAUCONITE PELLETS ON WHICH COMPOSITIONAL TRANSECTS HAVE BEEN DONE

	AM-04A		AM-04B		PG-07A		PG-1-2A		SB-03G		SB-PL	
	Ave.	σ	Ave.	σ	Ave.	σ	Ave.	σ	Ave.	σ	Ave.	σ
SiO <sub>2</sub> wt.%	51.77	0.75	52.69	0.66	52.07	0.74	53.14	1.14	50.87	0.73	50.18	0.97
TiO <sub>2</sub>	0.05	0.02	0.07	0.03	0.04	0.02	0.14	0.06	0.06	0.06	0.03	0.01
Al <sub>2</sub> O <sub>3</sub>	17.06	1.91	16.59	0.71	19.43	0.85	20.78	1.78	24.18	1.33	19.54	0.76
MgO	2.36	0.05	2.38	0.07	2.31	0.09	2.51	0.08	2.22	0.12	2.17	0.05
CaO	0.23	0.02	0.29	0.03	0.20	0.01	0.15	0.03	0.20	0.02	0.40	0.01
Fe <sub>2</sub> O <sub>3</sub>	12.97	1.71	12.17	0.77	10.38	0.54	9.13	0.71	7.31	0.94	11.19	0.41
FeO	2.95	0.39	2.76	0.17	2.36	0.12	2.08	0.16	1.66	0.21	2.54	0.09
Na <sub>2</sub> O	0.08	0.01	0.05	0.02	0.10	0.01	0.11	0.00	0.15	0.02	0.12	0.01
K <sub>2</sub> O	8.58	0.11	8.55	0.15	8.78	0.06	7.87	0.26	8.14	0.16	8.12	0.18

Each pellet has 10 analyzed points except for SB-PL with 5. Because of a relatively homogeneous composition, these averages will be considered as the composition for the pellets and used as such in mass-balance calculations.

TABLE 4. AVERAGE COMPOSITION OF GLAUCONITE ON THE BASIS OF ELECTRON-MICROPROBE ANALYSES

	AC-01E	AC-03A	AC-04A	AM-01B	AM-01E	AM-02C	AM-04A	AM-04B								
SiO <sub>2</sub> wt.%	53.80	50.96	51.96	53.67	54.51	53.24	55.60	52.78	53.68	55.60	55.86	55.16	52.95	54.27	52.84	52.51
TiO <sub>2</sub>	0.10	0.08	0.03	0.07	0.07	0.07	0.03	0.04	0.12	0.06	0.09	0.10	0.05	0.07	0.02	0.04
Al <sub>2</sub> O <sub>3</sub>	20.61	19.65	14.89	17.06	23.42	18.56	22.34	24.35	22.94	22.62	20.71	19.43	18.29	19.59	17.53	18.02
MgO	2.33	2.21	3.00	3.11	2.55	2.62	2.85	2.77	2.43	2.33	2.53	2.67	2.47	2.39	2.27	2.50
CaO	0.31	0.30	0.18	0.22	0.18	0.17	0.18	0.27	0.27	0.16	0.12	0.11	0.21	0.28	0.32	0.32
Fe <sub>2</sub> O <sub>3</sub>	9.38	8.93	12.60	11.13	6.41	10.29	7.52	8.23	6.68	6.92	8.63	9.19	11.27	11.82	11.76	11.82
FeO	2.13	2.16	2.86	2.53	1.46	2.34	1.71	1.87	1.52	1.57	1.96	2.09	2.56	2.36	2.67	2.69
Na <sub>2</sub> O	0.11	0.13	0.06	0.08	0.09	0.10	0.22	0.23	0.08	0.08	0.12	0.12	0.06	0.08	0.06	0.06
K <sub>2</sub> O	7.85	8.38	7.09	7.62	6.46	7.40	6.56	6.17	5.59	6.11	6.69	6.73	7.60	7.22	7.83	8.02
Total	96.66	93.56	92.75	95.52	95.18	94.87	97.05	96.67	93.32	95.47	96.69	95.59	95.47	98.09	95.31	96.03
Si <i>apfu</i>	3.57	3.53	3.65	3.64	3.58	3.61	3.61	3.45	3.59	3.64	3.66	3.67	3.60	3.57	3.61	3.57
<sup>IV</sup> Al	0.42	0.46	0.35	0.36	0.41	0.38	0.39	0.54	0.40	0.36	0.34	0.33	0.40	0.42	0.39	0.43
<sup>VI</sup> Al	1.19	1.14	0.89	1.00	1.40	1.10	1.32	1.34	1.40	1.39	1.26	1.20	1.06	1.09	1.02	1.01
Mg	0.23	0.23	0.31	0.31	0.25	0.27	0.28	0.27	0.24	0.23	0.25	0.26	0.25	0.23	0.23	0.25
Fe <sup>3+</sup>	0.47	0.50	0.67	0.57	0.32	0.53	0.37	0.41	0.34	0.34	0.43	0.46	0.58	0.59	0.60	0.60
Fe <sup>2+</sup>	0.12	0.13	0.17	0.14	0.08	0.13	0.09	0.10	0.08	0.09	0.11	0.12	0.15	0.13	0.15	0.15
Σ	2.01	2.00	2.05	2.04	2.05	2.03	2.05	2.11	2.07	2.04	2.03	2.04	2.03	2.04	2.01	2.03
Layer charge	-0.78	-0.86	-0.71	-0.75	-0.63	-0.73	-0.58	-0.59	-0.58	-0.50	-0.54	-0.61	-0.74	-0.70	-0.81	-0.80
Interlayer																
Ca	0.02	0.02	0.01	0.02	0.01	0.01	0.01	0.01	0.02	0.01	0.01	0.01	0.02	0.02	0.02	0.02
Na	0.01	0.02	0.01	0.01	0.01	0.01	0.03	0.01	0.01	0.01	0.01	0.01	0.02	0.01	0.01	0.01
K	0.66	0.74	0.64	0.66	0.54	0.64	0.54	0.51	0.48	0.51	0.56	0.57	0.66	0.61	0.68	0.70
Σ	0.70	0.78	0.67	0.69	0.57	0.67	0.58	0.56	0.51	0.53	0.58	0.59	0.68	0.64	0.71	0.73
Inter. charge	0.72	0.80	0.68	0.70	0.58	0.68	0.59	0.57	0.53	0.54	0.59	0.60	0.70	0.66	0.73	0.75

	PG-04H	PG-7A	PG-1-2A	SB-03G	SB-PL	Least altered <sup>1</sup>	GL-O <sup>2</sup>				
SiO <sub>2</sub> wt.%	53.63	54.51	52.65	54.11	54.76	52.44	51.91	51.57	51.92	50.44	50.9
TiO <sub>2</sub>	0.04	0.04	0.08	0.03	0.05	0.08	0.01	0.03	0.01	0.10	0.05
Al <sub>2</sub> O <sub>3</sub>	19.74	17.88	19.00	25.26	23.29	18.65	18.63	22.67	17.44	15.11	7.55
MgO	2.33	2.18	1.85	1.74	2.40	2.49	2.45	2.08	2.24	2.37	4.45
CaO	0.17	0.17	0.21	0.19	0.11	0.08	0.18	0.37	0.39	0.23	0.05
Fe <sub>2</sub> O <sub>3</sub>	9.99	10.90	11.48	6.72	8.13	11.28	11.54	9.95	13.51	14.48	17.20
FeO	2.27	2.48	2.61	1.53	1.85	2.56	2.62	2.26	3.07	3.29	2.20
Na <sub>2</sub> O	0.11	0.10	0.16	0.12	0.11	0.19	0.15	0.19	0.14	0.10	0.05
K <sub>2</sub> O	8.57	8.66	8.09	7.89	6.99	8.22	7.97	7.22	7.45	8.64	7.95
Σ	96.92	96.99	96.1	97.62	97.68	96.01	95.47	96.44	96.24	94.81	90.40
Si <i>apfu</i>	3.58	3.65	3.56	3.51	3.55	3.56	3.54	3.44	3.54	3.55	3.78
<sup>IV</sup> Al	0.42	0.35	0.43	0.49	0.45	0.44	0.45	0.56	0.46	0.44	0.22
<sup>VI</sup> Al	1.14	1.07	1.08	1.44	1.33	1.05	1.05	1.23	0.95	0.81	0.44
Mg	0.23	0.22	0.19	0.17	0.23	0.25	0.25	0.21	0.23	0.25	0.49
Fe <sup>3+</sup>	0.50	0.55	0.59	0.33	0.40	0.58	0.59	0.50	0.69	0.77	0.96
Fe <sup>2+</sup>	0.13	0.14	0.15	0.08	0.10	0.15	0.15	0.13	0.18	0.19	0.14
Σ	2.00	1.97	2.00	2.02	2.06	2.03	2.04	2.06	2.04	2.02	2.03
Layer charge	-0.78	-0.77	-0.78	-0.68	-0.60	-0.75	-0.77	-0.69	-0.72	-0.86	-0.76
Interlayer											
Ca	0.01	0.01	0.01	0.01	0.01	0.01	0.01	0.03	0.03	0.02	0.00
Na	0.01	0.01	0.02	0.01	0.01	0.02	0.02	0.02	0.02	0.01	0.01
K	0.73	0.74	0.70	0.65	0.58	0.71	0.69	0.61	0.65	0.78	0.75
Σ	0.76	0.76	0.74	0.68	0.60	0.74	0.73	0.67	0.69	0.81	0.76
Inter. charge	0.77	0.77	0.75	0.69	0.61	0.75	0.72	0.70	0.72	0.83	0.76

Samples are listed in ascending stratigraphic order. Two analyses were done per pellet to ascertain the extent of chemical variation within them. The Fe<sup>2+</sup>/Fe<sup>3+</sup> value determined by titration was applied to all samples. The number of cations was determined using 10 oxygen and 2 hydroxyl (22 charges). <sup>1</sup> is the composition showing the highest Fe<sub>total</sub> + Mg / <sup>VI</sup>Al value, and is used as the composition of the least altered grain in the mass-balance calculation. <sup>2</sup> is the composition of the standard GL-O, taken from Odin & Matter (1981).

Anse Maranda Formation is ferrian illite rather than glauconite.

On compositional graphs, ferrian illite from the Anse Maranda Formation plots in the same field as ferrian (or ferric) illite or aluminum-rich glauconite from other published studies (Fig. 3). A strong negative linear correlation between aluminum and iron contents (Figs. 3a, e) is evident for most of the samples, suggesting an aluminum-for-iron substitution at the octahedral site. A more significant relation, in determining the cause of the substitution, is the weak positive correlation between interlayer cations (mostly potassium, see Table 4) and iron (Figs. 3b, f). These relations suggest that the substitution of iron and magnesium by aluminum in glauconitic materials involves a potential loss in potassium (Figs. 3c, g). This relationship is explained by the release of divalent cations (iron and magnesium) and uptake of aluminum, therefore causing a decrease in layer charge and consequent expulsion of potassium. The high level of aluminum cannot be attributed to the presence of kaolinite or precursor grains, because their presence was not detected by X-ray diffraction (Fig. 2).

In conclusion, the amount of aluminum substituting for iron and magnesium seems to be more important than in previously reported studies of aluminum-rich glauconitic material. The relationship between potassium and iron is not related to the process of formation (Clauer *et al.* 1992, Odin & Matter 1981). Therefore, this unusual composition may help in understanding the true nature of such Al-rich glauconite and of some cases of ferrian illite.

#### EVALUATION OF POTASSIUM LOSS

Potassium content and crystallinity are used to determine glauconite maturity and the time of formation (Odin & Fullagar 1988). Consequently, potential changes in the potassium content during post-formational processes (diagenesis, weathering) will directly affect the interpretation of maturity and duration of evolution (Odin & Dodson 1982, Odin & Fullagar 1988). Therefore, it is critical to evaluate the importance of such post-depositional changes. This can be achieved through several steps.

Potassium loss, or gain, is obtained by means similar to hydrothermal mass-balance calculations (MacLean & Kranidiotis 1987). In this method, loss or gain of a given element is calculated using the values of an immobile element in the least altered sample (Ti for example). In the Anse Maranda Formation, alteration has affected all samples. Furthermore, the natural variability of glauconite composition makes it difficult to find an immobile element of constant concentration on which to base the calculation, and then to determine the substitution factor (the extent of Al for Fe + Mg substitution). Because we suggest that the Al for Fe + Mg substitution is related to diagenesis, the relative

intensity of diagenesis can be deduced from the  $(\text{Fe}_{\text{total}} + \text{Mg}) / {}^{\text{VI}}\text{Al}$  value; the sample with the highest value (or with the least substitution) can be considered as the least altered sample for mass-balance calculations. A sample from the AM-04A cross-section with a ratio of 1.49 is, thus, used as the least altered sample (Table 4). All samples have experienced the same burial history.

Assuming that aluminum was added during a post-depositional process, the  $(\text{Fe}_{\text{total}} + \text{Mg}) / {}^{\text{VI}}\text{Al}$  value of the samples must be brought to the value of the least altered material (1.49) by replacing aluminum with iron (divalent and trivalent) and magnesium. The number of cations added in the mass balance is defined by the slope of the correlation line on the interlayer cations *versus*  $\text{Fe}_{\text{total}} + \text{Mg}$  diagram (Figs. 3c, g). This diagram shows a slight positive linear correlation of 0.10, similar to the case for average Al-rich glauconite and ferrian illite. However, eight out of the 13 samples of ferrian illite from the Anse Maranda Formation show a steeper trend, at 0.41. Both figures are used for the corresponding samples in the following calculations.

The Al for Fe + Mg substitution induces a deficiency in layer charge. The amount of charge loss is given by the slope on Figures 3c and 3g. The 0.41 slope indicates that 1.0 octahedral aluminum for iron + magnesium substitution during diagenesis leads to the loss of 0.41 potassium atoms. Other interlayer cations are not considered because they are only minor constituents (Table 4). To produce a charge imbalance of 0.41, trivalent aluminum must replace 0.41 divalent (Mg and  $\text{Fe}^{2+}$ ) and 0.59 trivalent ( $\text{Fe}^{3+}$ ) cations at the octahedral site. To have a mass-balance calculation as precise as possible, the proportion of  $\text{Fe}^{2+}$  and Mg must be known. The -1.12 slope on Al *versus*  $\text{Fe}_{\text{total}}$  (Fig. 3a) indicates that the total amount of iron is not sufficient to substitute for all the aluminum on a 1:1 basis. An extra 0.12 Mg must also substitute for aluminum. Therefore, a loss of 0.12 Mg and 0.29  $\text{Fe}^{2+}$ , for a total of 0.41 divalent cations, is proposed for the present mass-balance. The lack of significant variations in Al and Si at tetrahedral sites in ferrian illite of the Anse Maranda Formation (Table 4) and in other studies (Odin & Matter 1981) suggests very little substitution. Therefore, no silica or tetrahedrally coordinated aluminum is added or subtracted during mass balance. Potassium is added according to the 0.41 ratio.

Because of the difficulty in rapidly obtaining the satisfactory  $(\text{Fe}_{\text{total}} + \text{Mg}) / {}^{\text{VI}}\text{Al}$  value through calculation, a curve was constructed in 0.05 increments in the Al for Fe + Mg substitution. Examples of two of such curves are given in Figure 4. To determine the correct substitution-factor for a given sample, one needs to determine the intersection of the calculated curve with the  $(\text{Fe}_{\text{total}} + \text{Mg}) / {}^{\text{VI}}\text{Al}$  value of the least altered sample. The substitution factor and corrected values of  $\text{K}_2\text{O}$  are given in Table 5.

The mass balance allows the reconstruction of the original, pre-alteration composition and variations in

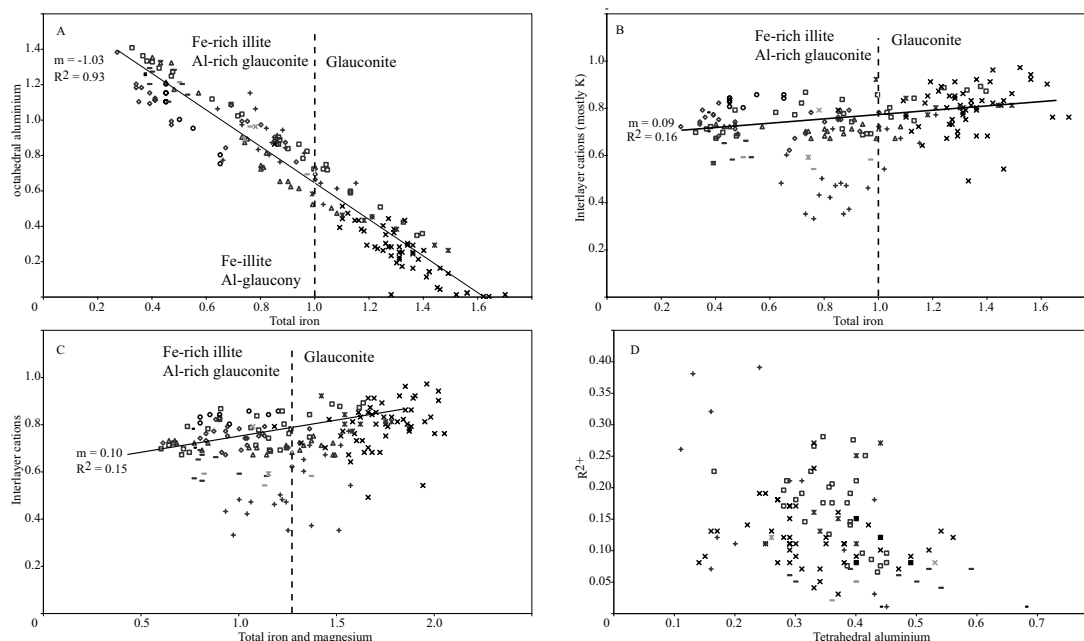


FIG. 3. Chemical composition of glauconitic minerals based on 10 atoms of oxygen and two hydroxyl groups formula and the division between iron-rich and aluminum-rich glauconite. A and E) Total iron *versus* octahedrally coordinated aluminum. The strong negative correlation between the two indicates an Al-for-Fe substitution. The  $-1.12$  slope indicates that aluminum also replaces other cations (Mg). B and F) The relation between total iron and interlayer cations (mostly potassium). There is no relation in the glauconite field, which accords with the model of glauconite formation. The weak relation for Al-rich glauconite and Fe-rich illite might suggest a post-formation loss in potassium. C and G) Total iron and magnesium *versus* interlayer cations. A generally poorly defined slope of  $0.10$  is visible for the majority of the samples. A steeper slope,  $0.41$ , is seen for some samples of the Anse Maranda Formation. These slopes are used in the evaluation of potassium loss. D and H) Lack of relation between tetrahedrally coordinated aluminum and divalent cations indicates that charge disequilibrium during Al-for-Fe substitution is neutralized by loss of potassium and not by the Al-Si substitution at tetrahedral sites.

composition (Fig. 5). Compositions of new glauconitic materials have iron values up to between 16.66% and 18.15%  $\text{Fe}_2\text{O}_3$  total (Table 5), which is closer to a conventional glauconite (Odin & Matter 1981). Differences in  $\text{K}_2\text{O}$  vary from a deficit of 2.02% to a gain of 0.35% (Table 5). Relative change in  $\text{K}_2\text{O}$  varies from 1.60% to 34.60%. However, only seven new values out of 12 show potassium variations greater than the standard deviation of their measured potassium.

In some cases, a minor Al for Fe total + Mg substitution results in an apparent gain in  $\text{K}_2\text{O}$  (sample AM-4B for example). This gain is due to the mass difference between iron and aluminum in expressing the mineral composition in percent. Also, the use of a 0.10 slope (overall slope; see Figs. 3c, g) in the mass balance would result in a very minor loss in potassium (Table 5, Fig. 5).

Mass-balance calculations indicate that there is a possibility of an apparent  $\text{K}_2\text{O}$  gain in glauconite with weak aluminum-for-iron substitution. A low value of  $\text{K}_2\text{O}$  (wt%) loss when using a 0.10 slope, and a differ-

ence in  $\text{K}_2\text{O}$  (wt%) lower than the standard deviation for ferrian illite of the Anse Maranda Formation with more than 13%  $\text{Fe}_2\text{O}_3$  (Fig. 6), could explain the "absence" of a potassium loss in previous studies.

## DISCUSSION

### *Aluminum-rich glauconite and causes of potassium loss*

The origin of aluminum-rich glauconite and of some ferrian illite, like those of the Anse Maranda Formation, is controversial. Aluminum-rich glauconite of alleged primary composition was described by Berg-Madsen (1983), Bjerkli & Ostmo-Sater (1973) and Keller (1958). The first case appears to have been exposed to weathering (fresh water, subaerial exposure) or diagenetic conditions, the second is clearly not glauconite but green pellets formed of several minerals, and the third is found in the fossil-rich, terrestrial to estuarine Morrison Formation. Others have proposed that the high

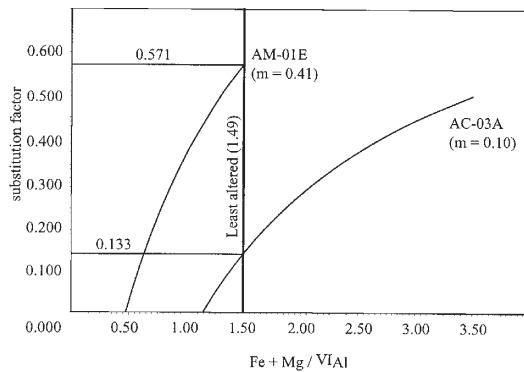
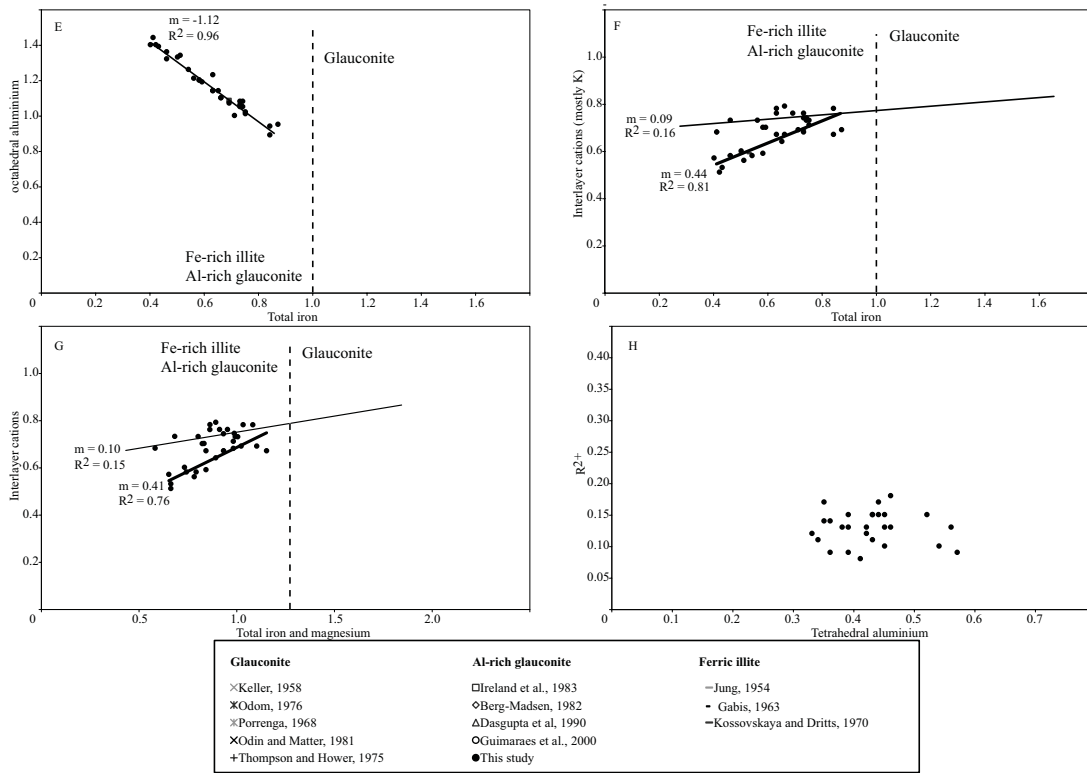


TABLE 5. COMPARISON OF MEASURED POTASSIUM AND RECONSTRUCTED POTASSIUM VALUES

Sample	m	Meas. K <sub>2</sub> O wt. %	St. dev. K <sub>2</sub> O wt. %	Substitution factor	New K <sub>2</sub> O wt. %	Diff. in K <sub>2</sub> O wt. %	Relative K <sub>2</sub> O %	New Fe <sub>2</sub> O <sub>3</sub> wt. %
AC-01E (2)	0.1	8.11	0.37	0.365	7.98	-0.13	-1.60	17.53
AC-03A (2)	0.1	7.36	0.37	0.133	7.23	-0.13	-1.78	16.69
AC-04A (2)	0.41	6.93	0.67	0.440	8.32	1.39	20.05	16.66
AM-01B (2)	0.41	6.36	0.28	0.490	7.88	1.52	23.82	16.73
AM-01E (2)	0.41	5.85	0.37	0.571	7.87	2.02	34.60	16.98
AM-02C (3)	0.41	7.20	0.85	0.405	8.39	1.19	16.52	16.71
AM-04A (3)	0.41	7.80	0.70	0.235	8.30	0.50	6.45	17.23
AM-04B (3)	0.1	8.13	0.37	0.192	7.88	-0.25	-3.09	17.47
PG-04H (2)	0.1	8.62	0.06	0.303	8.26	-0.35	-4.07	17.42
PG-07A (3)	0.1	8.26	0.47	0.405	8.03	-0.23	-2.73	18.15
PG-01-2A (2)	0.41	7.43	0.62	0.445	8.67	1.24	16.71	16.89
SB-03G (3)	0.41	8.11	0.13	0.335	9.00	0.89	10.96	17.02
SB-PL (3)	0.41	7.59	0.47	0.263	8.24	0.64	8.46	17.67

FIG. 4. Variation of the substitution factor versus the  $(Fe + Mg) / VIAl$  value. The 1.49 value is the one from the reference material, e.g., the least modified glaucouitic mineral (AM-04A). Curves for other samples are determined by reconstructing the mineral composition using a different substitution-factor (extent of Al-for-Fe substitution). The substitution-factor used for final reconstruction is the one that corresponds to the  $(Mg + Fe) / VIAl$  value of the reference material.

Number in bracket next to the sample number is the number of pellets used for the average composition. The slope (m) used for mass balance depends on where the sample plots on Figure 3c. Some are close to the 0.1 slope, others, to the 0.41 slope. Substitution factor is determined from calculations, as in Figure 4. New % K<sub>2</sub>O is the result obtained from a mass-balance calculation. Diff. in K<sub>2</sub>O is the difference between the Measured K<sub>2</sub>O and New K<sub>2</sub>O. Relative loss in K<sub>2</sub>O, expressed in %, is equal to 100 (Diff. in K<sub>2</sub>O (in wt.%) / Measured K<sub>2</sub>O (in wt.%)). A negative value means a gain of potassium expressed as weight %, even though the process leads to a loss in potassium, expressed as cation per half unit cell.

aluminum content is of diagenetic origin (Dasgupta *et al.* 1990, Guimaraes *et al.* 2000, Ireland *et al.* 1983). Some iron-rich illite has a similar composition, but its formation is related to hypersaline or fluvial environments (Dasgupta *et al.* 1990, Gabis 1963, Hay *et al.* 1991, Jung 1954, Kossovskaya & Drits 1970, Parry & Reeves 1966, Porrenga 1968). This is not the case for the Anse Maranda Formation (Longu  p  e & Cousineau 2005). Iron-rich illite of diagenetic origin also has been identified (Deb & Fukuoka 1998, Huggett *et al.* 2001).

According to Burst (1958), glauconitic minerals form from degraded layer silicates by uptake of potassium and iron. This "layer lattice" theory suggests a relation between iron and potassium contents. However, this model of formation has been rejected for several reasons (Odin & Matter 1981, Odom 1984). In the "verdissement" or "neo-formation" model, glauconitic minerals can form from different precursor grains (Odin & Matter 1981, Odom 1976). This process has been later defined as a two-fold process in which potassium and iron are incorporated at different stages (Clauer *et al.* 1992). The different timing between iron and potassium intake explains the lack of correlation between potassium and iron for (true) glauconite observed by Odin & Matter (1981), Odom (1984) and in Figure 3b. Because the models of Odin & Matter (1981) and Clauer *et al.* (1992) do not include a positive linear relation between iron and potassium (or negative aluminum – potassium relation), the iron – potassium relationship visible in Figures 3b and 3f for Al-rich glauconite and ferrian illite must be related to post-formation processes (*e.g.*, weathering, metamorphism and diagenesis).

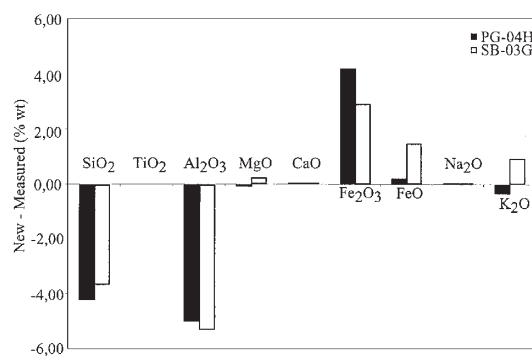


FIG. 5. Difference in composition (wt %) in glauconitic minerals after mass balance for the PG-04H and SB-03G samples. The substitution factor is about the same for both samples (Table 4), but the slope ( $m$ ) used is different. There was no silica removed during mass balance. The apparent loss is due to mass difference between iron and aluminum. This difference also results in an apparent loss in potassium for PG-04H, even though potassium was added.

Weathering is an important agent in post-formation changes in glauconite composition. The most common product of weathering of glauconite is goethite, formed by the removal of iron. This process seems to be active on the seafloor (Odin & Fullagar 1988), or during subaerial exposure (Huggett & Gale 1997). However, chemical analysis of such weathered glauconite results in a high iron value because goethite is trapped in the micropores within the glauconitic pellet. Slightly weathered glauconite shows no indication of potassium loss, whereas highly weathered pellets ( $> 50$  wt% Fe) no longer contain potassium and show aluminum and silica loss as well (Huggett & Gale 1997). The ferrian illite of the Anse Maranda Formation does not exhibit any of these weathering-induced signatures. No goethite or other iron oxides, for that matter, are visible within or around the pellet, except for hematite in a 10-m interval near the top of the 355 m-thick formation. Weathering of glauconite causes the 001 reflection to move from 10 to 11   (Odin & Rex 1982). This has not happened for the Anse Maranda material. Finally, the outcrops show no evidence of intense weathering, and the geological evolution of the Anse Maranda Formation does not involve exhumation before recent time.

Burial diagenesis of glauconite in a reducing environment causes iron to be replaced by aluminum while the expelled iron forms pyrite (Ireland *et al.* 1983). In their study, Ireland *et al.* (1983) reported that a decrease in layer charge caused by  $Al^{3+}$  substituting for  $Mg^{2+}$  and  $Fe^{2+}$  in the layer of octahedra is balanced by an  $Al^{3+}$  for  $Si^{4+}$  substitution in the tetrahedral site. No significant change in interlayer composition takes place. Such charge balancing cannot be seen on a plot of divalent cations *versus*  $IVAl$  (Figs. 3d, h). Also, the Anse Maranda Formation glauconite-bearing sandstones contain virtually no pyrite (less than 0.1% S). Hematite is the only non-silicate iron-bearing mineral found, and

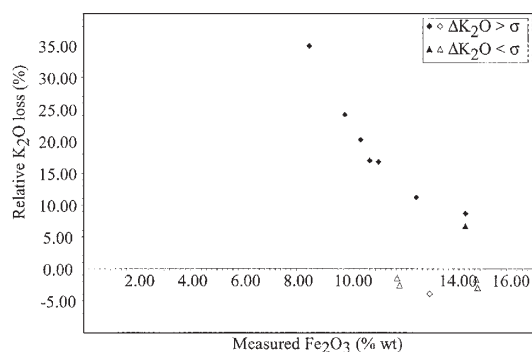


FIG. 6. Graphs illustrating the necessity of correcting potassium content. Samples with less than 13% measured iron generally have relative loss in potassium greater than the standard deviation. This could explain, in part, the "absence" of potassium loss in previous studies.

its distribution is limited to red sandstones near the top of the formation, or to a few crystals in the green sandstones. An alternative sink for iron is the chloritization of feldspar. Under reducing, neutral or acid conditions, microcline and albite may be replaced by chlorite and quartz by incorporation of  $\text{Fe}^{2+}$  and Mg and the release of K (Morad & Aldahan 1987). In this model, the iron and magnesium are derived from biotite, whereas the released potassium is fixed in illite. The Anse Maranda sandstones show diagenetic chlorite – albite – illite – quartz and detrital feldspar – quartz – biotite (altered to chlorite) assemblages with glauconitic mineral as a possible source of iron. Still, the whereabouts of the lost iron is a problem for the Anse Maranda Formation glauconitic mineral. Whereas chloritization of feldspar appears to take place in the sandstones of the Anse Maranda Formation, as suggested by micrometric chlorite partially replacing feldspar grains, it is unlikely to be a significant sink for the iron because the process takes place during deep burial (Morad & Aldahan 1987, Ogunyomi 1980). Ferrian illite found within early-cemented burrows and host sandstones of the Anse Maranda Formation has a similar iron content, which means that iron loss happened before the early cementation of calcite. Therefore, the timing of the iron loss suggests that diagenesis of glauconite can occur during early burial. The other possible iron sink is the coarse-grained chlorite (Fig. 1b) found in both the burrows and the host sediment. The almost complete alteration of feldspar grains, the high intensity of bioturbation, and the high content of clays in the glauconitic sediments are similarities between the Anse Maranda Formation and the Cretaceous Lower Greensand Group from the Isle of Wight (McCarty *et al.* 2004). These authors do not, however, link the dissolution of feldspar to the glauconitization process. Some of their glauconite is Al-rich, which might suggest that feldspar could be the source for Al, and that the whole process was triggered by bioturbation. A sink for potassium (illite) and iron (nontronite) is present (McCarty *et al.* 2004).

The lack of other iron-bearing minerals in the Anse Maranda Formation can be explained by 1) intense upward circulation of water that causes iron to be expelled in solution, or 2) minor loss in iron, in which case the ferrian illite is primary. The occurrence of an early chlorite mixed with the late diagenetic one has to be considered. Velde & Odin (1975) mentioned that regardless of potassium content, glauconitic pellets are surrounded by a thin outer zone of aluminum-rich glauconite. This supports the early timing of the diagenesis. This trend, although not as obvious, can be detected in the Anse Maranda Formation ferrian illite (Table 2). The difference between a rimmed and whole aluminum-rich pellet might be due to the intensity of diagenesis or time over which early diagenesis was active, or to porosity in the grain of glauconite.

So far, the process that led to the aluminum-iron substitution in glauconitic pellets from the Anse

Maranda Formation is unknown, but several elements point to an early diagenetic process in which the composition of the host sediment and bioturbation may have had a role to play.

#### Impact on glauconite maturity

A slight change in the potassium value leads to a major difference in the interpreted time of evolution, especially for glauconite with high potassium content (Fig. 7). The variations in the duration of evolution would eventually cause miscalculation of rates of sedimentation (given more refinement of the model of glauconite formation). Change in potassium content can also lead to misinterpretation when using K content of glauconite in a sequence-stratigraphy framework (Amorosi & Centineo 2000).

In the Anse Maranda Formation, the least evolved glauconite (*i.e.*, the ferrian illite with the lower potassium; sample AM-01E) is found near the base of the formation, corresponding to a time at which the sea level was high (Longuépée & Cousineau 2005), and the glauconite maturity increases with sea-level fall. This is in contradiction to the current understanding of the process of formation of glauconite (Amorosi 1995, Odin & Fullagar 1988). Using the new potassium value (Table 5), the difference between the lower and upper parts of the formation is reduced. This is in better accordance with the depositional model for the Anse Maranda Formation (Longuépée & Cousineau 2005). The use of the measured  $\text{K}_2\text{O}$  content of the ferrian illite contradicts the depositional model, but not the new values of  $\text{K}_2\text{O}$ . This is an example of how a failure to recognize the diagenetic nature of the ferrian illite and Al-rich glauconite composition could lead to bias in interpretation of relative sea-level changes and sediments influx.

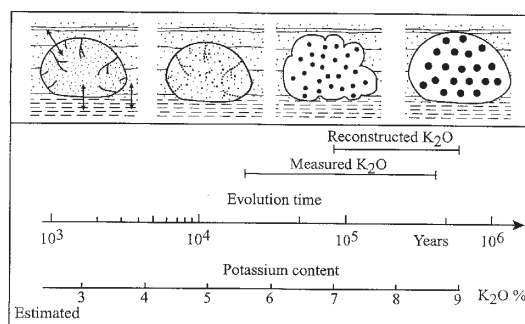


FIG. 7. Effect of potassium loss on the evaluation of the duration of evolution. The time scale and grain morphology were defined by Odin & Dodson (1982). Note that reconstruction tends to narrow the range of potassium value. This can be attributed to the technique of recalculation, and also to a stable sedimentary environment.

### *Impact on isotopic studies*

An isotopic study of the Anse Maranda ferrian illite was not performed. Thus we do not have data to compare with other studies. The Rb–Sr system has yielded information regarding the process of formation of glauconite (Clauer *et al.* 1992) and also for dating (Clauer 1982), but the K–Ar and, recently,  $^{39}\text{Ar}$ – $^{40}\text{Ar}$  are the favored techniques in geochronology for such materials. However, not all glauconite can be used for such analysis. Because of inherited argon, only mature glauconite (>6%  $\text{K}_2\text{O}$ ) can be used (Odin & Fullagar 1988). Recrystallization during diagenesis and metamorphism causes argon loss (Odin *et al.* 1977). Another problem is that argon recoil during heating leads to argon loss from small particles (Brereton 1972). This problem has, however, been reduced by the development of new analytical procedures (Dong *et al.* 1995, Smith *et al.* 1993). Hassanipak & Wampler (1997) also suggested that composition is the major factor in argon loss, rather than particle size. The loss of potassium during early diagenesis, as suggested by our data, can also prove to be a problem, because it can lead to an underestimation of the radiogenic argon formed, depending on the timing of the closure. Using the K–Ar method, the loss of potassium will inevitably cause glauconite to yield older ages, unless the mineral releases the same proportion of radiogenic argon. However, the aluminum-for-iron substitution might help the retention of argon. It has been demonstrated by Killingley & Day (1990) and Levy (1990) that dehydroxylation, which helps the release of argon, occurs at lower temperature for iron-rich clay minerals compared to aluminum-rich ones because the Al–OH bond is stronger than the Fe–OH bond. As glauconite might be closed to potassium before, or soon after, burial (Odin & Dodson 1982) and as the process leading to the aluminum-for-iron substitution also occurs early, the effect of the latter on radiometric age might be minimal. Because the K–Ar can vary in so many ways in accordance with so many processes, it is difficult to assess how the proposed early diagenesis would influence the system. Even though early diagenesis might prove insignificant, it has to be accounted for in radiometric dating or diagenetic studies using K–Ar or Ar–Ar data (Aronson & Hower 1976, Weaver & Wampler 1970) and as a factor potentially influencing the zero age (Odin & Dodson 1982).

### CONCLUSIONS

Glauconite from the Cambrian Anse Maranda Formation is an Al-rich glauconitic mineral, as is glauconite from several other locations throughout the world. It has lower values of iron and magnesium relative to more conventional compositions of glauconite. Even if the mineral can better be classified as an iron-rich illite, it retains the morphological habits and optical properties of a glauconite, and was formed in

an environment where the formation of glauconite was likely to occur. Because of the strong environmental significance of both minerals and of the diagenetic nature of the Anse Maranda Formation glauconite, it would be misleading, at least for a sedimentologist, to call this mineral ferrian illite. The term (peraluminous) glauconite or glaucony-derived ferrian illite seems more appropriate.

A linear positive correlation between the contents of aluminum and total iron indicates Al-for-Fe substitution at the octahedral site. This substitution causes a loss in potassium that can be observed on interlayer cations *versus* iron (*i.e.*, K – Fe) diagram for the glauconite. Corrections for potassium loss were applied to the Anse Maranda Formation data through a calculation using a mass-balance method and using the sample with the highest (Fe + Mg) /  $^{VI}\text{Al}$  value as the reference material. These new potassium values represent change between –1.60 and +34.60% of their measured values. The changes translate to no more than 2.02 wt%  $\text{K}_2\text{O}$ . The lack of a relationship between interlayer cations and iron reported in previous studies can be interpreted as due to 1) the lower slope of the linear correlation between these elements (relative to this study), 2) the apparent gain of  $\text{K}_2\text{O}$  (expressed in wt%) even with the removal of K (expressed in number of cations), and 3) a variation in potassium within pellets greater than potassium loss ( $\text{K}_2\text{O}$  wt%) for (peraluminous) glauconite with more than 13% measured  $\text{Fe}_2\text{O}_3$  total.

Existing models for glauconite formation and weathering do not provide sufficient explanation for the Al-rich composition of (peraluminous) glauconite. Although the exact conditions are unknown, diagenesis appears to be the most likely process by which glauconite loses its potassium. Other diagenetic features of the Anse Maranda Formation suggest that the chemical changes occurred early on during burial, or even at the sea bottom. The nature of the substrate and bioturbation may have an influence on the process. The incoming of an acid hydrothermal fluid could also be a factor. In the case of the Anse Maranda Formation, the iron sink is not resolved, but a closer look at the chlorite might yield more information in that regard.

The potassium content of glauconite is used to determine its maturity and to evaluate the time required for its formation. Failing to recognize potassium loss would lead to misinterpretations of variations in sea level in sequence stratigraphy and of the environment of deposition. The loss has a major effect on evaluating the time of glauconite evolution and, therefore, would affect the possible calculation of a rate of sedimentation. The chemical change could be a problem in interpreting isotopic data for either dating or diagenetic studies, because of potassium loss and an unknown behavior of argon during this process. We therefore recommend an evaluation of the diagenetic change in glauconite using major oxide compositions before venturing into isotopic studies.

## ACKNOWLEDGEMENTS

This work is part of Geological Survey of Canada NATMAP – Geological Bridges of Eastern Canada project. Dr. Denis Lavoie, the main contact at the Geological Survey of Canada, was of great help in all the aspects of the project. We are grateful to Dr. A. Amorosi from the University of Bologna and Dr. A. Chagnon from the Institut National de la Recherche Scientifique for providing insights on methodology. The paper was improved following reviews by Drs. A.E. Lalonde, J. Środoń and R.F. Martin. The project was financially supported by a National Sciences and Engineering Research Council operating grant (OGP0037226) to PAC and a Petro-Canada bursary to HL.

## REFERENCES

- AMOROSI, A. (1993): *Intérêt des niveaux glauconieux et volcano-sédimentaires en stratigraphie: exemple de dépôts de bassins tectoniques miocènes des Apennins et comparaison avec quelques dépôts de plate-forme stable*. Ph.D. thesis, Université Pierre et Marie Curie, Paris, France.
- AMOROSI, A. (1995): Glaucony and sequence stratigraphy: a conceptual framework of distribution in siliciclastic sequences. *J. Sediment. Res.* **B65**, 419-425.
- AMOROSI, A. (1997): Detecting compositional, spatial and temporal attributes of glaucony: a tool for provenance research. *Sediment. Geol.* **109**, 135-153.
- AMOROSI, A. & CENTINEO, M.C. (2000): Anatomy of a condensed section: the Lower Cenomanian glaucony-rich deposits of Cap Blanc-Nez (Boulonnais, northern France). In *Marine Authigenesis: from Global to Microbial*. Soc. Econ. Paleontol. Mineral., Spec. Publ. **66**, 405-414.
- ARONSON, J.L. & HOWER, J. (1976): Mechanism of burial metamorphism of argillaceous sediment. 2. Radiogenic argon evidence. *Geol. Soc. Am., Bull.* **87**, 738-744.
- BAILEY, S.W., ALIETTI, A., BRINDLEY, G.W., FORMOSA, M.L.L., JASMUND, K., KONTA, J., MACKENZIE, R.C., NAGASAWA, K., RAUSSELL-COLOM, R.A. & ZVYAGIN, B.B. (1980): Summary of the recommendations of the AIPEA nomenclature committee. *Clays Clay Minerals* **28**, 73-78.
- BERG-MADSEN, V. (1983): High-alumina glaucony from the middle cambrian of Öland and Bornholm, southern Baltoscandia. *J. Sediment. Petrol.* **53**, 875-893.
- BJERKLI, K. & OSTMO-SÆTER, J.V. (1973): Formation of glauconie in foraminiferal shells on the continental shelf off Norway. *Marine Geology* **14**, 169-178.
- BRERETON, N.R. (1972): A reappraisal of the  $^{40}\text{Ar}$ - $^{39}\text{Ar}$  stepwise degassing technique. *R. Astronom. Soc., Geophys. J.* **27**, 449-478.
- BURST, J.F. (1958): Mineral heterogeneity in glauconite pellets. *Am. Mineral.* **43**, 481-497.
- CLAUER, N. (1982): The rubidium–strontium method applied to sediments: certitudes and uncertainties. In *Numerical Dating in Stratigraphy*. John Wiley and Sons, Chichester, U.K. (245-276).
- CLAUER, N., KEPPENS, E. & STILLE, P. (1992): Sr isotopic constraints on the process of glauconitization. *Geology* **20**, 133-136.
- DASGUPTA, S., CHAUDHURI, A.K. & FUKUOKA, M. (1990): Compositional characteristics of glauconitic alterations of K-feldspar from India and their implications. *J. Sediment. Petrol.* **62**, 277-281.
- DEB, S.P. & FUKUOKA, M. (1998): Fe-illites in a Proterozoic deep marine slope deposit in the Penganga Group of the Pranhita Godavari Valley: their origin and environmental significance. *J. Geol.* **106**, 741-749.
- DONG, H., HALL, C.M., PEACOR, D.R. & HALLIDAY, A.N. (1995): Mechanism of argon retention in clays revealed by laser  $^{40}\text{Ar}$ - $^{39}\text{Ar}$  dating. *Science* **267**, 355-359.
- GABIS, V. (1963): Étude minéralogique et géochimique de la série sédimentaire oligocène du Velay. *Bull. Soc. fr. Minéral. Cristallogr.* **86**, 315-354.
- GUIMARAES, E.M., VELDES, B., HILLIER, S. & NICOT, E. (2000): Diagenetic/anchimetamorphic changes on the Proterozoic glauconite and glaucony from the Paranoa Group mid-western Brazil. *Revista Brasileira de Geociências* **30**, 363-366.
- HASSANIPAK, A.A. & WAMPLER, J.M. (1997): Radiogenic argon release by stepwise heating of glauconite and illite: the influence of composition and particle size. *Clays Clay Minerals* **44**, 717-726.
- HAY, R.L., GULDMAN, S.G., MATTHEWS, J.C., LANDER, R.H., DUFFIN, M.E. & KYSER, T.K. (1991): Clay mineral diagenesis in core KM-3 in Searles Lake, California. *Clays Clay Minerals* **39**, 84-96.
- HELSELBO, S.P. & HUGGETT, J.M. (2001): Glaucony in ocean-margin sequence stratigraphy (Oligocene–Pliocene, offshore New Jersey, U.S.A.; ODP leg 174A). *J. Sediment. Res.* **71**, 599-607.
- HUGGETT, J.M. & GALE, A.S. (1997): Petrology and palaeoenvironmental significance of glaucony in the Eocene succession at Whitecliff Bay, Hampshire Basin, UK. *J. Geol. Soc. London* **154**, 897-912.
- HUGGETT, J.M., GALE, A.S. & CLAUER, N. (2001): The nature and origin of a non-marine 10 Å clay from the late Eocene and early Oligocene of the Isle of Wight (Hampshire Basin), UK. *Clay Minerals* **36**, 447-464.
- IRELAND, B.J., CURTIS, C.D. & WHITEMEN, J.A. (1983): Compositional variation within some glauconites and illites and implications for their stability and origins. *Sedimentology* **30**, 769-786.
- JUNG, J. (1954): Les illites du bassin oligocène de Saline (Cantal). *Bull. Soc. fr. Minéral. Cristallogr.* **77**, 1231-1238.

- KELLER, W.D. (1958): Glauconitic mica in the Morrison Formation in Colorado. *In* National Conference on Clays and Clay Minerals. *National Research Council, Mem.* **566**, 120-128.
- KILLINGLEY, J.S. & DAY, S.J. (1990): Dehydroxylation kinetics of kaolinite and montmorillonite from Queensland Tertiary oil shale deposits. *Fuel* **69**, 1145-1149.
- KOSSOVSKAYA, A.G. & DRITS, V.R. (1970): Micaceous minerals in sedimentary rocks. *Sedimentology* **15**, 83-101.
- LAMBOY, M. (1976): *Géologie marine du plateau continental au N.O. de l'Espagne*. Thèse de doctorat, Université de Rouen, Rouen, France.
- LEVY, J.H. (1990): Effect of water pressure on the dehydration and dehydroxylation of kaolinite and smectite isolated from Australian Tertiary oil shales. *Energy Fuels* **4**, 146-151.
- LONGUÉPÉE, H. & COUSINEAU, P.A. (2005): Reappraisal of the Cambrian glauconite-bearing Anse Maranda Formation, Québec Appalachians: from deep-sea turbidites to clastic shelf deposits. *Can. J. Earth Sci.* **42**, 259-272.
- MACLEAN, W.H. & KRANIDIOTIS, P. (1987): Immobile elements as monitor of mass transfer in hydrothermal alteration: Phelps Dodge massive sulfide deposit, Matagami, Quebec. *Econ. Geol.* **82**, 951-962.
- MCCARTY, D.K., DRITS, V.R., SAKHAROV, B., ZVIAGINA, B.B., RUFFELL, A. & WACH, G. (2004): Heterogeneous mixed-layer clays from the Cretaceous Greensand, Isle of Wight, southern England. *Clays Clay Minerals* **52**, 552-575.
- MCCRACKEN, S.R., COMPTON, J. & HICKS, K. (1996): Sequence-stratigraphic significance of glaucony-rich lithofacies at site 903. *In* Proc. Ocean Drilling Program, Scientific Results. Ocean Drilling Program, College Station, Texas.
- MOORE, D.M. AND REYNOLDS, R.C., JR. (1989): *X-ray Diffraction and the Identification and Analysis of Clay Minerals*. Oxford University Press, Oxford, U.K.
- MORAD, S. & ALDAHAN, A.A. (1987): Diagenetic chloritization of feldspars in sandstones. *Sediment. Geol.* **51**, 155-164.
- ODIN, G.S. & DODSON, M.H. (1982): Zero isotopic age of glauconies. *In* Numerical Dating in Stratigraphy. John Wiley and Sons, Chichester, U.K. (277-306).
- ODIN, G.S. & FULLAGAR, P.D. (1988): Geological significance of the glaucony facies. *In* Green Marine Clays. Elsevier, Amsterdam, The Netherlands (295-332).
- ODIN, G.S. & LETOLLE, R. (1980): Glauconitization and phosphatization environments; a tentative comparison. *In* Marine Phosphorites; Geochemistry, Occurrence, Genesis. *Soc. Econ. Paleontol. Mineral., Spec. Publ.* **29**, 227-237.
- ODIN, G.S. & MATTER, A. (1981): De glauconiarum origin. *Sedimentology* **28**, 611-641.
- ODIN, G.S. & REX, D.C. (1982): Potassium-argon dating of washed, leached, weathered and reworked glauconies. *In* Numerical Dating in Stratigraphy. Wiley, Chichester, U.K. (363-386).
- ODIN, G.S., VELDE, B. & BONHOMME, M. (1977): Radiogenic argon in glauconites as a function of mineral recrystallization. *Earth Planet. Sci. Lett.* **37**, 154-158.
- ODOM, E.I. (1976): Microstructure, mineralogy and chemistry of Cambrian glauconite pellets and glauconite, central U.S.A. *Clays Clay Minerals* **24**, 232-238.
- ODOM, E.I. (1984): Glauconite and celadonite minerals. *In* Micas (S.W. Bailey, ed.). *Rev. Mineral.* **13**, 545-584.
- OGUNYOMI, O. (1980): *Diagenesis and Deep-Water Depositional Environments of Lower Paleozoic Continental Margin Sediments in the Quebec City Area, Canada*. Ph.D. thesis, McGill University, Montreal, Quebec.
- PARRY, W.T. & REEVES, C.C. (1966): Lacustrine glauconitic mica from pluvial lakes, Mound Lynn and Terry counties, Texas. *Am. Mineral.* **51**, 229-235.
- PORRENGA, D.H. (1968): Non-marine glauconitic illite in the Lower Oligocene of Aardenburg, Belgium. *Clay Minerals Bull.* **7**, 421-429.
- RIEDER, M., CAVAZZINI, G., D'YAKONOV, Y.S., FRANK-KAMENETSKII, V.A., GOTTARDI, G., GUGGENHEIM, S., KOVAL, P.V., MÜLLER, G., NEIVA, A.M.R., RADOSLOVICH, E.W., ROBERT, J.-L., SASSI, F.P., TAKEDA, H., WEISS, Z. & WONES, D.R. (1998): Nomenclature of the micas. *Can. Mineral.* **36**, 905-912.
- RUFFELL, A. & WACH, G. (1998): Firmgrounds – key surfaces in the recognition of parasequences in the Aptian Lower Greensand Group, Isle of Wight (southern England). *Sedimentology* **45**, 91-107.
- SMITH, P.E., EVENSON, N.M. & YORK, D. (1993): First successful <sup>40</sup>Ar-<sup>39</sup>Ar dating of glauconies: argon recoil in single grains of cryptocrystalline material. *Geology* **21**, 41-44.
- THOMPSON, G.R. & HOWER, J. (1975): The mineralogy of glauconite. *Clays Clay Minerals* **23**, 289-300.
- VELDE, B. & ODIN, G.S. (1975): Further information related to the origin of glauconite. *Clays Clay Minerals* **23**, 376-381.
- WEAVER, C.E. & WAMPLER, J.M. (1970): K, Ar, illite burial. *Geol. Soc. Am., Bull.* **81**, 3423-3430.
- WHIPPLE, E.R. (1974): A study of Wilson's determination of ferrous iron in silicates. *Chem. Geol.* **14**, 223-238.
- WILSON, A.D. (1955): A new method for the determination of ferrous iron in rocks and minerals. *Geol. Surv. Great Britain, Bull.* **9**, 56-58.

Received November 22, 2004, revised manuscript accepted August 3, 2005.